

# Creep behaviour and microstructure evolution of advanced creep-resistant 9%Cr martensitic steels under cyclic thermal loading

V. Sklenička<sup>1,2\*</sup>, K. Kuchařová<sup>1</sup>, M. Svoboda<sup>1,2</sup>

<sup>1</sup>*Institute of Physics of Materials, Academy of Sciences of the Czech Republic, 616 62 Brno, Czech Republic*

<sup>2</sup>*CEITEC – Institute of Physics of Materials, Academy of Sciences of the Czech Republic, 616 62 Brno, Czech Republic*

Received 3 January 2018, received in revised form 24 January 2018, accepted 25 January 2018

## Abstract

The effect of cyclic thermal loading on the creep behaviour and microstructure evolution of three creep strength enhanced 9%Cr ferritic-martensitic steels (P91, P92 and E911) was investigated. The temperature cycles consisted of cooling the specimen after creep exposure from the creep testing temperature of 600 °C to room temperature and then heating it up again to the creep testing temperature. Standard creep tests at the same creep testing temperature were carried out simultaneously for comparison. The results of the thermal cycled and standard creep tests showed no detrimental effect of intermittent heating on the creep behaviour of the specimens during the cycled tests. Microstructural investigations revealed no substantial differences in the types and chemical compositions of precipitating phases for the specimens after standard or cyclic creep in the three steels examined. There is no reason to expect substantially different creep behaviour for specimens experiencing standard or cyclic creep, provided that the specimens possess similar microstructures.

**Key words:** 9%Cr creep-resistant steels, cyclic thermal loading, creep, microstructure evolution, precipitation, fractography

## 1. Introduction

New and emerging energy technologies are of great interest. However, coal power plants continue to make a considerable contribution to energy requirements into the foreseeable future. Since the electricity generated by renewables (e.g. solar, wind) can suddenly disappear, standby conventional power plants have to start-up very rapidly [1, 2]. It should be noted that most coal power plants are specifically designed for base load duty, and operate in creep conditions most efficiently when the load and temperature remain constant over time [3, 4]. Thus, we can expect that the cumulative effects of frequently repeated thermal and load cycling from repeated plant start-ups and shut-downs may result in the accumulation or acceleration of creep damage.

Creep deformation processes and microstructure evolution during high-temperature creep of advanced 9%Cr martensitic creep-resistant steels have been

widely reported over the last two decades [5–14]. At the same time, extensive experimental microstructural analyses and thermodynamic modelling of microstructure evolution and stability during high-temperature creep of these steels have also been published [6–8, 12, 13, 15–18]. The effect of cyclic loading, which is commonly found under service conditions, is of special relevance. Cyclic thermal creep and creep-fatigue interaction are possible causes of the damage and failure of high-temperature components under cycling loading. Intensive efforts have recently been undertaken to study the role of the high-temperature cyclic behaviour on creep strength enhanced 9%Cr steels [19–32]. The effect of hold time and stress ratio at a constant temperature on cyclic creep properties of advanced 9%Cr steels was investigated in most of these studies. However, there is currently insufficient information regarding the effect of cyclic intermittent heat events on the high-temperature deformation and microstructure stability of these steels.

---

\*Corresponding author: e-mail address: [sklen@ipm.cz](mailto:sklen@ipm.cz)

The cyclic operation has become a frequent operation regime for both old conventional plants and new combined cycle plants [2]. It should be recognised that cyclic operation represents a wide range of modes and combinations, starting with two-shifting, in which the plant undergoes start-up and shutdown once a day, and ending with the sporadic operation for periods of less than two weeks followed by the shutdown for more than several days [33]. The common mode of operation is weekend shutdown in which the plant shuts down at weekends.

Periodic applications of intermittent heat events are normally absent when creep-resistant steels are evaluated. Thus, the primary objectives of the present paper are to obtain some information on the effect of cyclic heating on both the creep behaviour and microstructure evolution of three creep strength enhanced 9%Cr ferritic-martensitic steels (namely P91, P92 and E911), and to simulate the weekend shutdown mode of plant operation which has many cycles of heating and cooling.

## 2. Materials and experimental procedures

### 2.1. Steels

The **P91** (ASME Gr.91) steel samples were produced by Vitkovice Steel a.s., Czech Republic, and subjected to the following two-stage heat treatment: 1060 °C/1 h/air + 750 °C/2 h/air. Its chemical composition is (in wt.%): 0.09 C, 0.56 Mn, 0.20 Si, 0.021 P, 0.009 S, 0.05 Cu, 0.46 Ni, 8.36 Cr, 0.86 Mo, 0.20 V, 0.06 Nb, 0.065 N and 0.007 Al. The **P92** (ASTM Gr.92) steel was produced by Nippon Steel Corporation, Japan, and received in the form of a seamless pipe with an outer diameter of 390 mm after the following heat treatment: 1060 °C/1 h/air + 770 °C/2 h/air. Its chemical composition is (in wt.%): 0.115 C, 8.85 Cr, 0.20 Si, 0.50 Mn, 0.017 P, 0.002 S, 0.24 Ni, 0.96 Mo, 0.22 V, 0.07 Nb, 1.8 W, 0.084 N and 0.007 Al. Finally, the **E911** steel primarily developed from the research work of the European cooperation action COST501 [34, 35], and was received after the following heat treatment: 1060 °C/1 h/air + 770 °C/2 h/air. Its chemical composition is (in wt.%): 0.11 C, 8.85 Cr, 0.96 Mo, 0.95 W, 0.22 V, 0.07 Nb, 0.08 N, 0.50 Mn, 0.20 Si, 0.02 P and 0.24 Ni.

### 2.2. Creep testing

Constant load tensile creep tests were carried out in an argon atmosphere. The effect of temperature variation during the creep test has been investigated by intermittent heating under constant load (Fig. 1). The creep specimens in the first cycle were heated

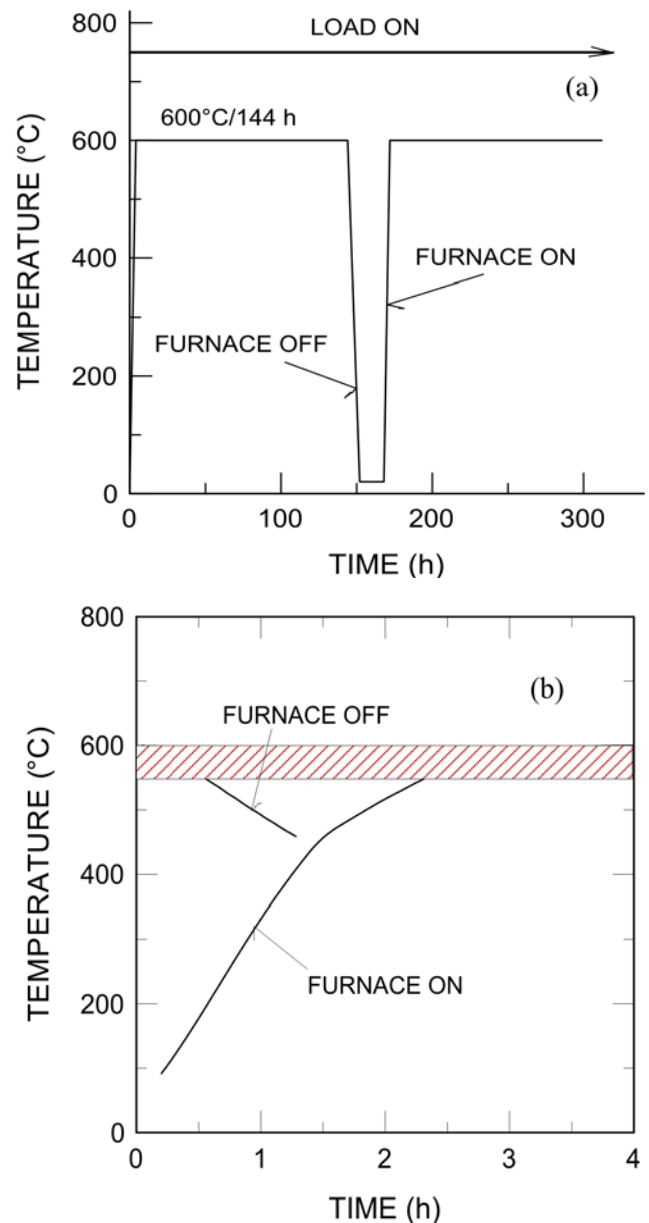


Fig. 1. Schematic illustration of intermittent heating sequences for a constant load cyclic creep test: (a) cyclic heating during creep exposure, (b) time behaviour of creep furnace.

from room temperature to the testing temperature, then creep loaded (the holding time at the testing temperature was about 144 h) and finally cooled to room temperature. This temperature cycling was repeated after 24 h, and then further repeated until the specimen underwent failure. Standard smooth creep tests at the same creep testing temperature and applied stress were performed simultaneously for comparison. The initial load (tensile stress) was maintained during the entire test in all cases.

Flat creep specimens with a gauge length of 50 mm

and a cross-sectional area of  $5 \text{ mm} \times 3.2 \text{ mm}$  were used in the tests. The creep testing was conducted at  $600^\circ\text{C}$  with the testing temperature maintained to within  $\pm 0.5^\circ\text{C}$  of the desired value. The creep elongations were continuously measured during creep exposure using a linear variable differential transducer.

### 2.3. Microstructural and fractographic investigations

Microstructure characterisation and fractographic analysis of the tested specimens were performed by means of transmission and scanning electron microscopy. Transmission electron microscopy (TEM) studies were carried out on carbon extraction replicas and foils prepared from both the grip and gauge parts of the creep specimens using a Philips CM12 TEM/SEM microscope equipped with the EDAX Phoenix system. Particles of secondary phases extracted into carbon replicas were identified by means of selected area diffraction (SAED), and their local chemical compositions were measured by energy dispersive X-ray spectroscopy (EDS), using a 10 nm probe size and thin sample approximation. A Tescan Lyra 3 XMU scanning electron microscope (SEM) was used for the fractographic investigation.

### 2.4. Thermodynamic calculations

Microstructure stability modelling should include predictions of the phase stability, nucleation rates, growth rates and coarsening rates for precipitate phases as functions of chemical composition, temperature and stress [36]. The CALPHAD type calculations [37] provide useful guidelines for the evaluation of the stable phases in the steels under investigation, based only on their chemical compositions. A series of equilibrium phase diagrams for P91, P92 and E911 steels, which show the calculated equilibrium mole fractions and coexisting phases as a function of temperature, have been produced.

## 3. Experimental results

### 3.1. Creep results

Two creep elongations  $\varepsilon$  versus time  $t$  creep curves for P91 steel, with different loading histories under the same applied uniaxial stress  $\sigma$  of 125 MPa, are shown in Fig. 2a. The first curve ( $T = \text{constant}$ ) represents the standard creep test, which was run at a constant load and a testing temperature of  $600^\circ\text{C}$  until the specimen fractured. The second curve in Fig. 2a shows the creep behaviour of the specimen with intermittent heating, resulting in the fracture of the specimen after 67 heat cycles. A clearer comparison of these

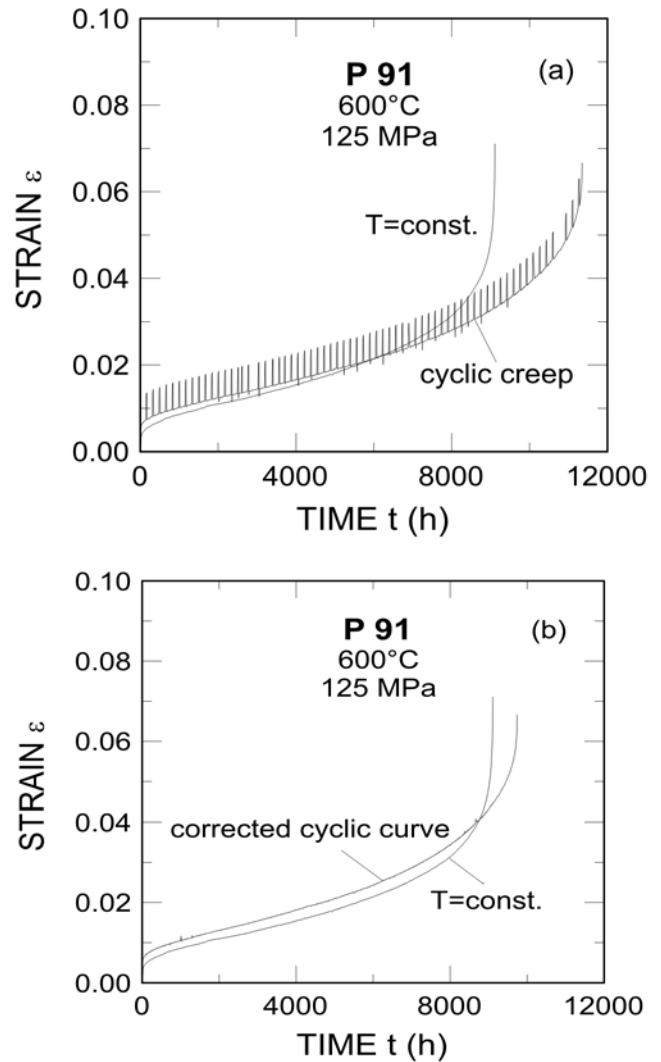


Fig. 2. Creep curves at 125 MPa for P91 steel with different loading histories: (a) uncorrected standard curve, (b) corrected curve.

two creep curves follows from Fig. 2b, where the creep curve for non-monotonic (cyclic) creep encompasses the time at the testing temperature only. The results of cycled and standard creep tests for P92 and E911 are shown in Figs. 3 and 4, respectively, for the same testing temperature and applied stress of 150 MPa. As shown in these figures, the cycled specimens failed after 77 cycles (P92 steel) and 107 cycles (E911 steel), respectively. Mutual comparison of the creep curves for E911 steel in Figs. 4 and 5 may indicate that different levels of applied stress affect the degree of cyclic creep.

### 3.2. Microstructure characterisation

The three steels exhibited similar tempered martensitic microstructures after creep exposure. The

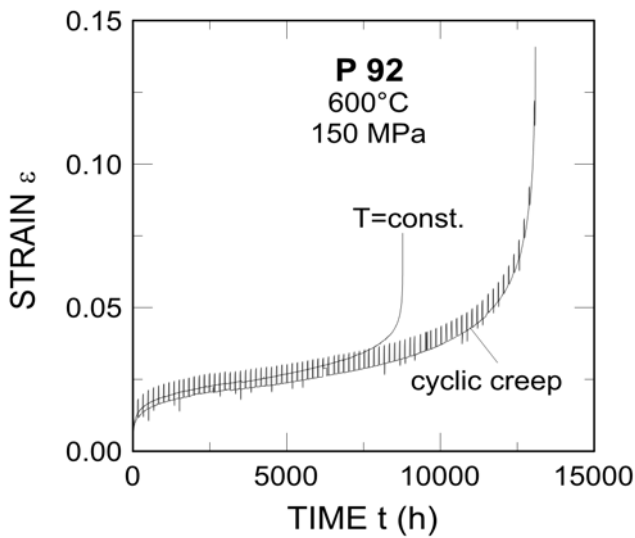


Fig. 3. Creep curves at 150 MPa for P92 steel with different loading histories.

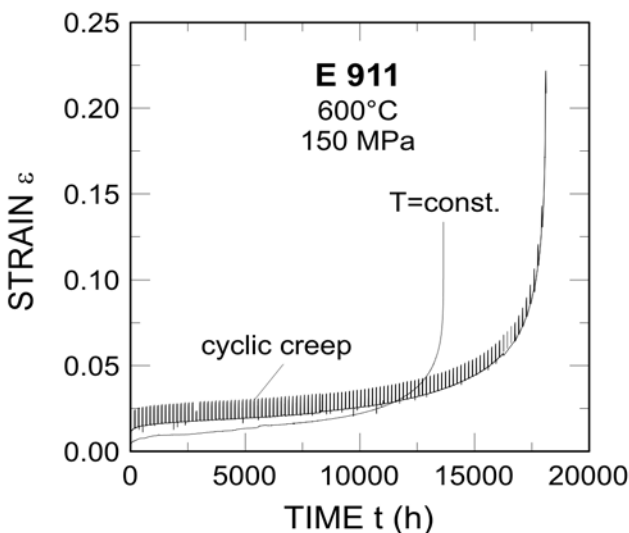


Fig. 4. Creep curves at 150 MPa for E911 steel with different loading histories.

microstructure of P91 steel is documented by the TEM micrographs in Fig. 6. The prior austenite grain boundaries are decorated by a network of  $M_{23}C_6$  particles. Particles of this phase are also observed on both the subgrain boundaries and inside the subgrains. Furthermore, there are tiny minor phase precipitates, present on both the grain boundaries and former martensitic laths. Careful examination also revealed very small particles inside martensitic laths.

A similar situation was found for the P92 and E911 steels and documented in their respective TEM micrographs (Figs. 7 and 8). Clearly defined subgrains are evident in both the grip area and gauge length

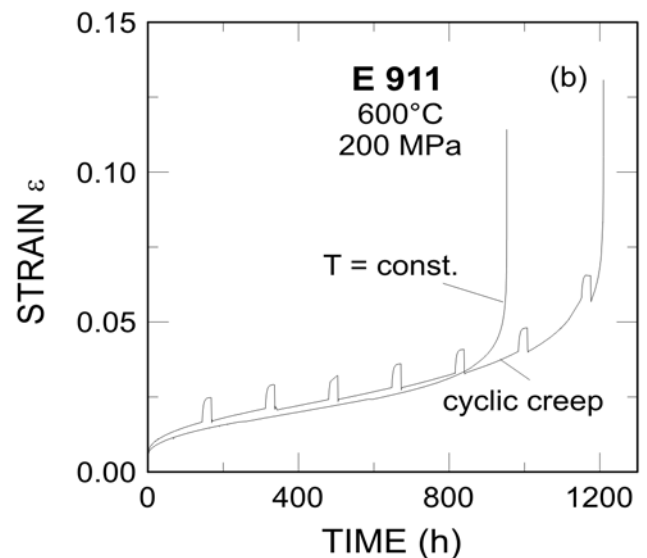
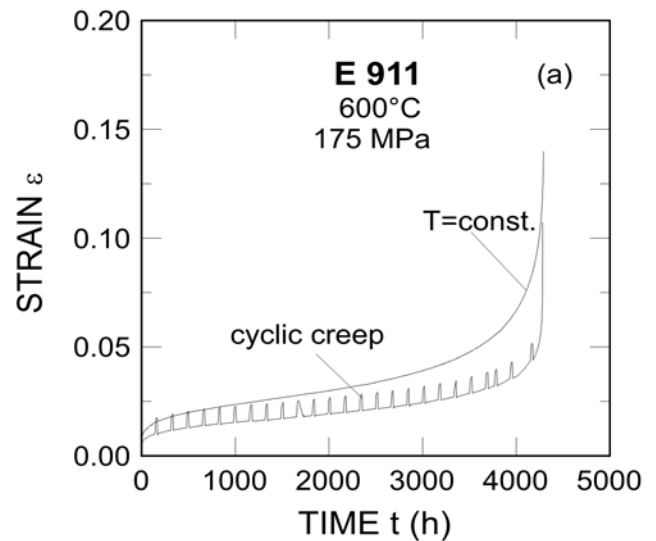


Fig. 5. Creep curves for E911 steel under different levels of applied stress: (a) 175 MPa, (b) 200 MPa.

of the test pieces. However, subgrain coarsening during creep exposure seems to be more intensive in the specimens that underwent creep at a constant testing temperature (monotonic creep) in comparison to the specimens whose growth in the gauge length is more pronounced than the growth in the grip location, suggesting that this growth is also influenced by stress. An increase in the subgrain shape is observed simultaneously with subgrain size growth, indicating that the subgrains tend to approach the equiaxed shape. Again, the rate of shape change is strongly influenced by the applied stress.

### 3.3. Precipitation analysis

It is possible to calculate the expected amounts and

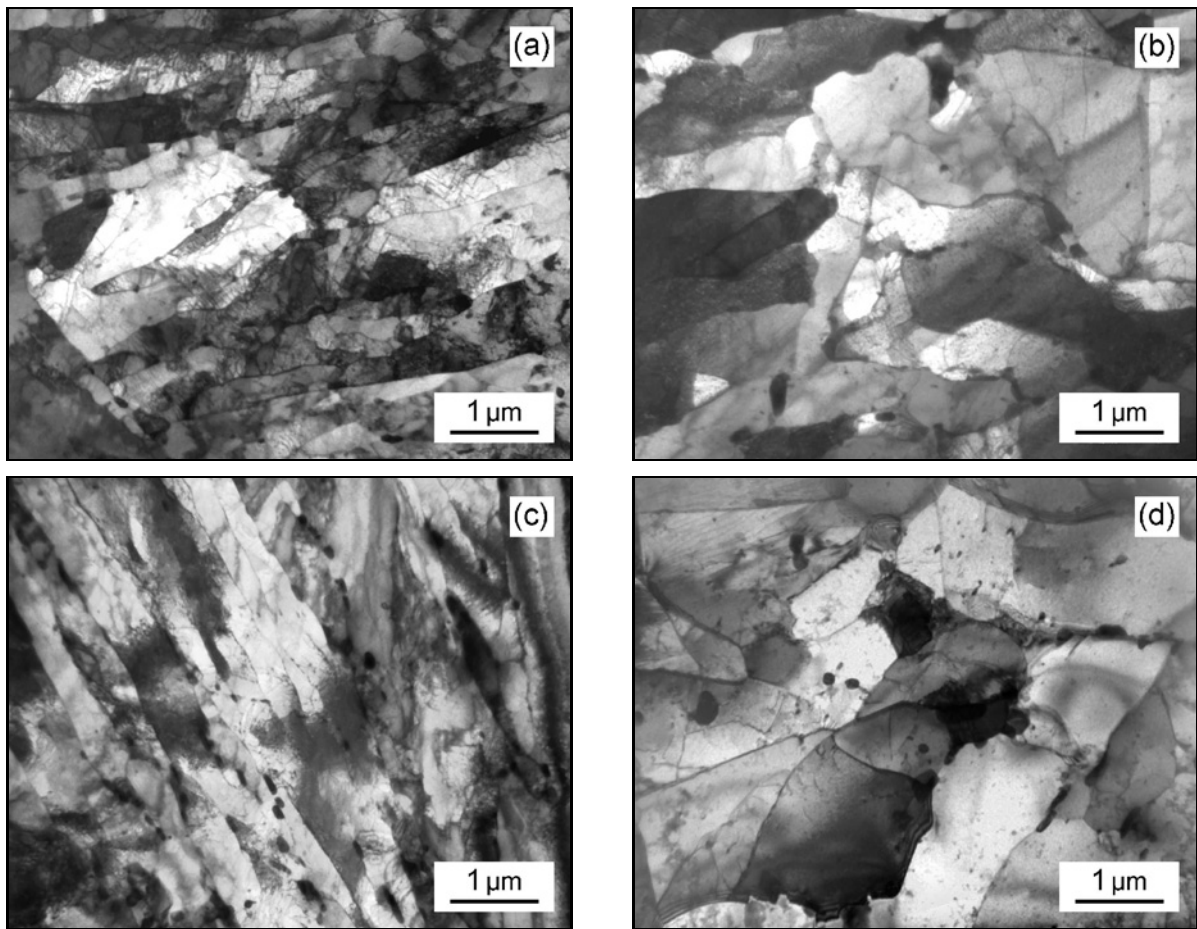


Fig. 6. TEM micrographs of P91 steel subjected to monotonic creep at 125 MPa: (a) grip location, (b) gauge length location, and cyclic creep at 125 MPa: (c) grip location, (d) gauge length location.

Table 1. Experimentally determined chemical composition (in at.%) of secondary phases in P91 steel after creep at 600 °C

P91	Phase	V	Cr	Mn	Fe	Nb	Mo
Monotonic creep	M <sub>23</sub> C <sub>6</sub>	1.9	54.2	1.3	15.9	0.7	5.3
	Laves	2.8	12.9	1.5	46.2	2.0	34.7
	MX	32.0	8.2	0.3	0.5	8.2	0.9
Cyclic creep	M <sub>23</sub> C <sub>6</sub>	1.6	54.2	1.2	17.5	0.6	4.2
	Laves	1.0	16.8	1.3	45.5	1.6	33.8
	MX	34.7	8.2	0.2	0.4	6.0	0.6

compositions of the precipitated coexisting secondary phases from the thermodynamic equilibrium calculation in the Thermocalc software (see Section 2.4). The series of equilibrium phase diagrams for P91, P92 and E911 in Figs. 9, 10 and 11, respectively, show the calculated mass fraction of the coexisting secondary phases and temperature dependence on phase composition.

The results of the direct microstructure investigations of the precipitated phases by electron microscopy show reasonably good agreement with the thermody-

Table 2. Experimentally determined chemical composition (in at.%) of secondary phases in P92 steel after creep at 600 °C

P92	Phase	V	Cr	Mn	Fe	W	Nb	Mo
Monotonic creep	M <sub>23</sub> C <sub>6</sub>	1.3	53.6	1.1	17.9	3.2	0.6	1.7
	Laves	2.3	17.1	1.3	41.1	26.6	2.1	9.5
	MX	35.5	6.7	0.3	0.9	0.5	5.6	0.5
	NbX	0.0	0.0	0.4	0.7	0.4	47.4	1.1
Cyclic creep	M <sub>23</sub> C <sub>6</sub>	1.4	52.3	0.7	17.6	4.0	1.0	2.3
	Laves	2.3	14.2	1.0	41.5	27.4	2.6	10.9
	MX	34.7	7.4	0.3	1.0	0.4	5.4	0.8
	NbX	4.9	2.9	0.6	1.1	1.8	37.8	0.9

amic calculations. The TEM micrographs in Figs. 12, 13 and 14 show the ascertained particle precipitation after monotonic and cyclic creep exposures for the three steels under investigation.

The quantitative TEM results of precipitated phases obtained by means of SAED and EDS are presented in Tables 1, 2 and 3. Collectively, the microstructures in all the steels contain three types of precipitates: M<sub>23</sub>C<sub>6</sub> (mostly coarse Cr carbides),

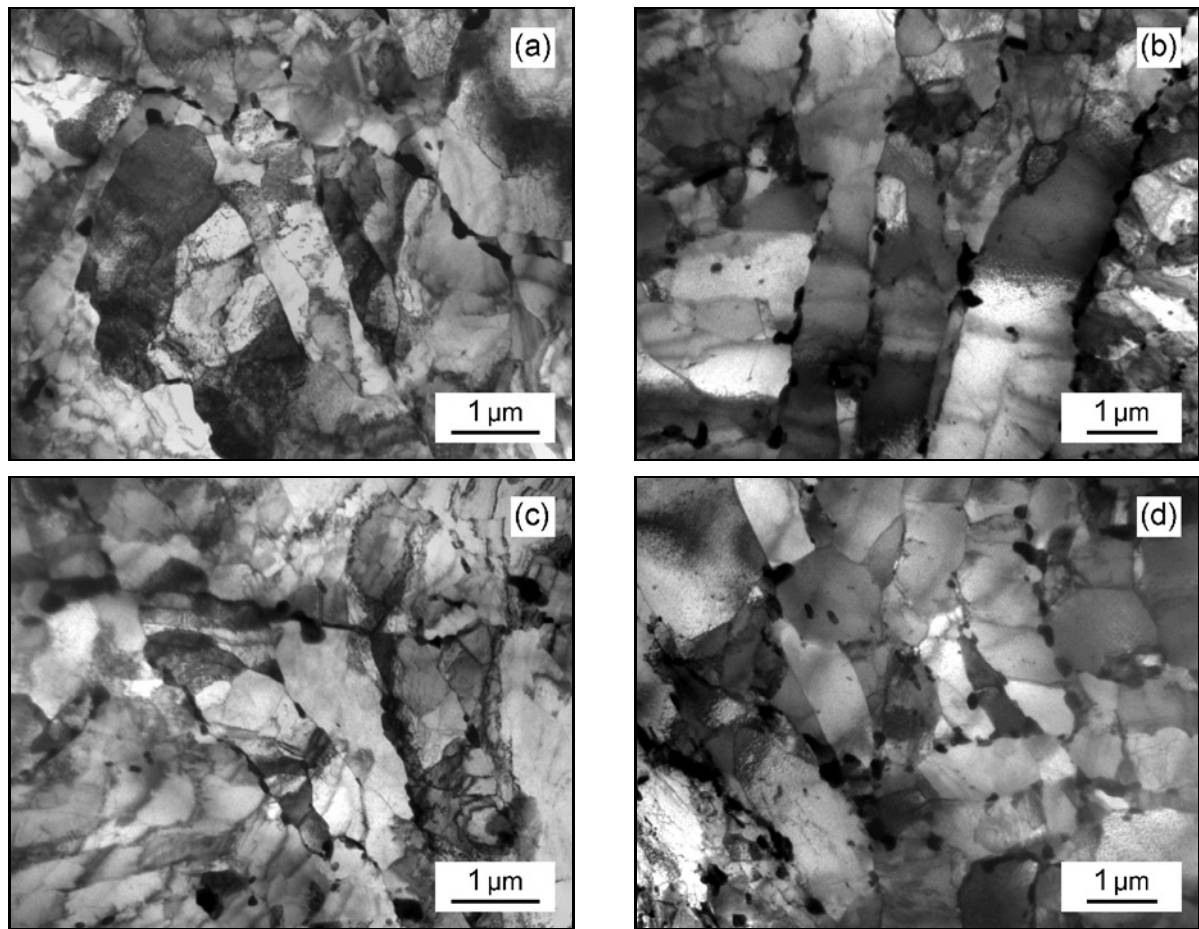


Fig. 7. TEM micrographs of P92 steel subjected to monotonic creep at 150 MPa: (a) grip location, (b) gauge length location, and cyclic creep at 150 MPa: (c) grip location, (d) gauge length location.

Table 3. Experimentally determined chemical composition (in at.%) of secondary phases in E911 steel after creep at 600 °C

P92	Phase	V	Cr	Mn	Fe	W	Nb	Mo
Monotonic creep	M <sub>23</sub> C <sub>6</sub>	2.3	55.8	0.9	14.2	0.1	0.8	5.1
	Laves	0.8	18.2	1.3	44.3	0.5	1.6	3.3
	MX	35.2	8.4	0.2	0.0	0.0	5.4	0.9
Cyclic creep	M <sub>23</sub> C <sub>6</sub>	1.3	57.0	0.9	14.6	0.1	0.5	4.9
	Laves	0.9	16.7	1.0	45.1	0.6	1.5	34.1
	MX	36.0	8.1	0.4	0.8	0.0	3.7	0.9

Laves phase (containing Mo in P91 and E911 steels and W + Mo in P92 steel) and precipitation of the MX type (M = V, Cr, Nb, Fe, Mo and X = N, C, prevailing form is fine V nitrides).

It can be concluded that there are no substantial differences between the types and chemical compositions of the precipitated phases for specimens after monotonic or cyclic creep in the three steels examined. The Laves phase precipitates are significantly smaller

in P92 steel compared to the P91 and E911 steels. No Z-phase precipitates [13, 38, 39] were experimentally identified perhaps due to short-term creep exposures.

### 3.4. Fractography

Upon examining the creep fracture surfaces of the investigated steels using SEM microscopy (Fig. 15), it was found that the fracture was always of the ductile dimple transgranular mode, regardless of the creep loading history. Creep cavities [8, 40] were observed to a limited extent, mainly in the fractured specimens of P92 steel and independent of the creep testing method. This was likely due to localised plastic deformation during the late tertiary stage of creep. Most of the cavities were observed in proximity to the fracture surface. A higher number of cavities occurred at coarse Laves phase precipitates.

## 4. Discussion

As demonstrated in Figs. 2–5, no clear detrimental effect of intermittent cyclic heating on the creep

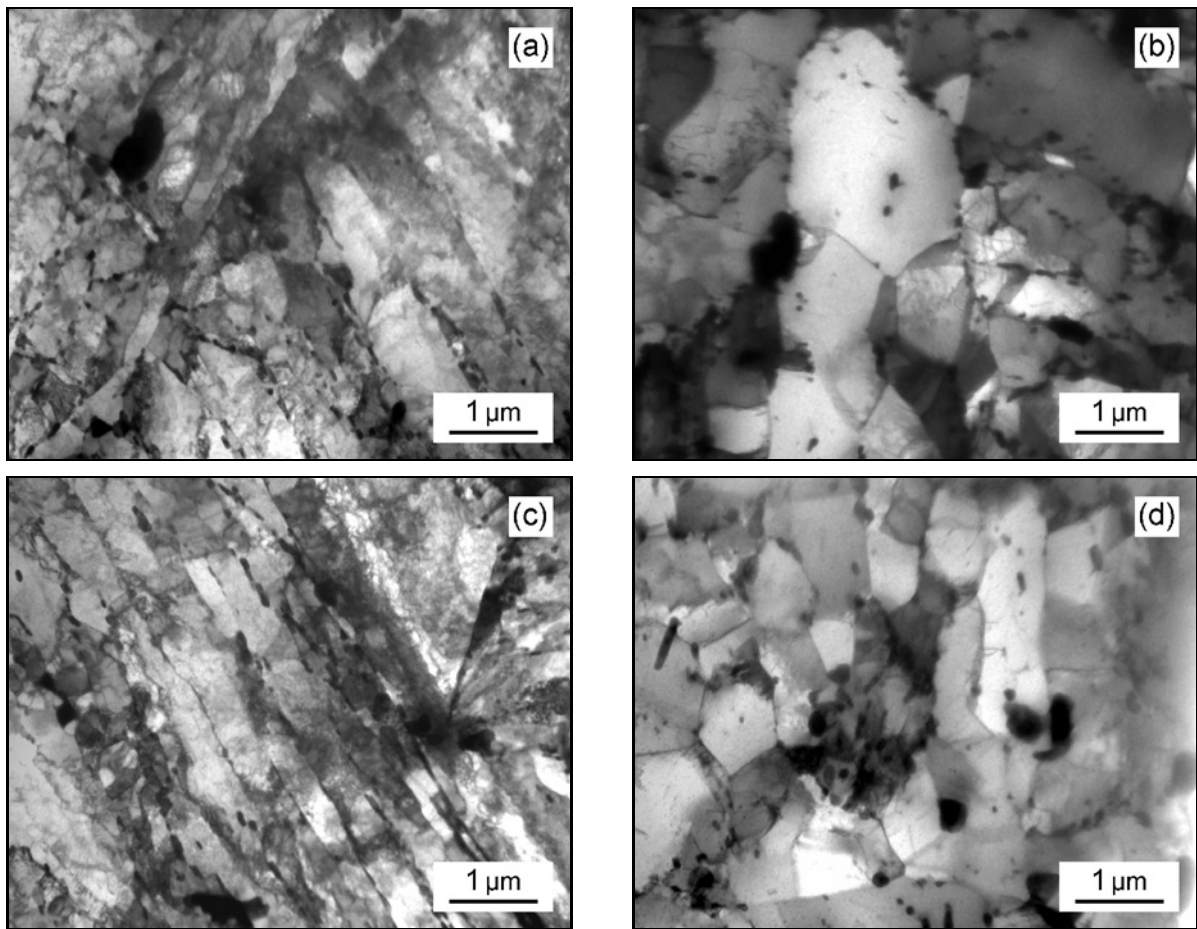


Fig. 8. TEM of E911 steel subjected to monotonic creep at 150 MPa: (a) grip location, (b) gauge length location, and cyclic creep at 150 MPa: (c) grip location, (d) gauge length location.

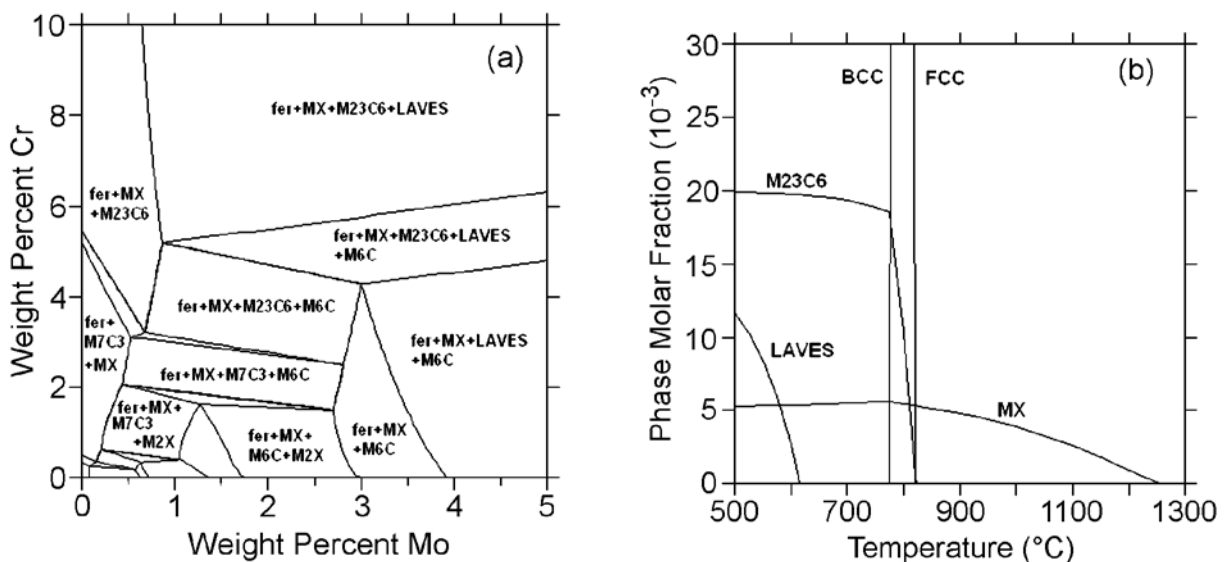


Fig. 9. The equilibrium phase diagrams for P91 steel: (a) mass fractions of secondary phases at 600°C, (b) temperature dependence on phase composition.

behaviour of the specimen during the cycled tests was found. The cycled specimens exhibit slightly longer

times to fracture than the specimens that underwent creep at a constant testing temperature, as can be seen

Table 4. Fracture times for the standard (monotonic) creep test,  $t_f$ , and cyclic creep,  $t_{fc}$ , and corrected time,  $t_{fccorr}$ , for cyclic creep at 600°C and various applied stresses

Steel	$\sigma$ (MPa)	$t_f$ (h)	$t_{fc}$ (h)	$t_{fccorr}$ (h)	$t_{fccorr}/t_f$
P91	125	9111	11350	9742	1.07
P92	150	8773	13088	11240	1.28
E911	150	13647	18120	15552	1.14

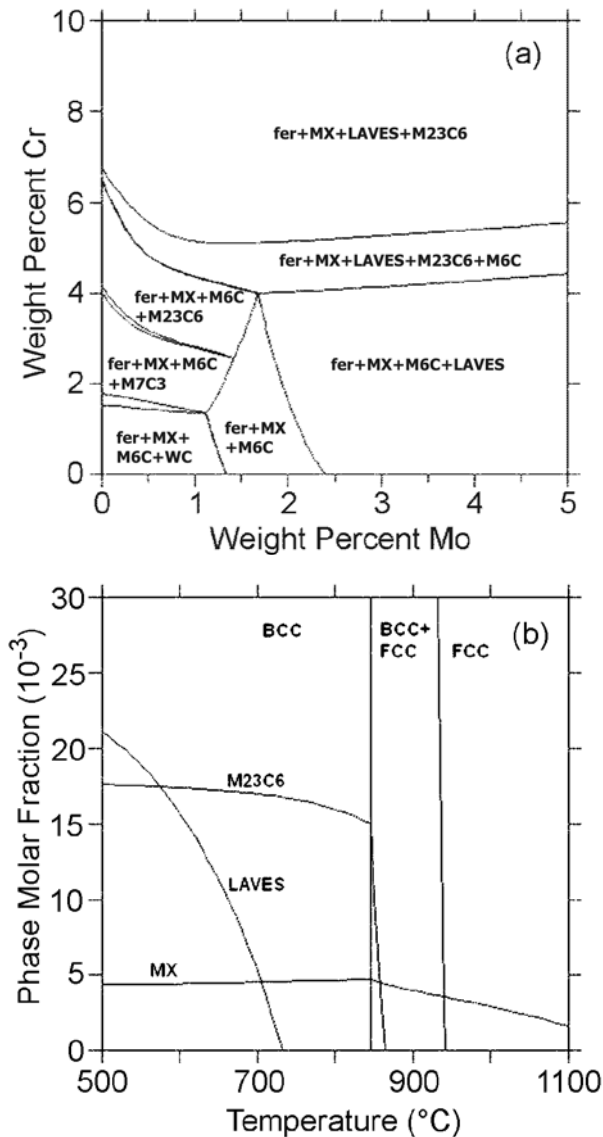


Fig. 10. The equilibrium phase diagrams for P92 steel: (a) mass fractions of secondary phases at 600°C, (b) temperature dependence on phase composition.

from Table 4. Here,  $t_f$  is the fracture time for the standard (monotonic) creep test,  $t_{fc}$  is the fracture time for cyclic creep (i.e., the total time of test exposure)

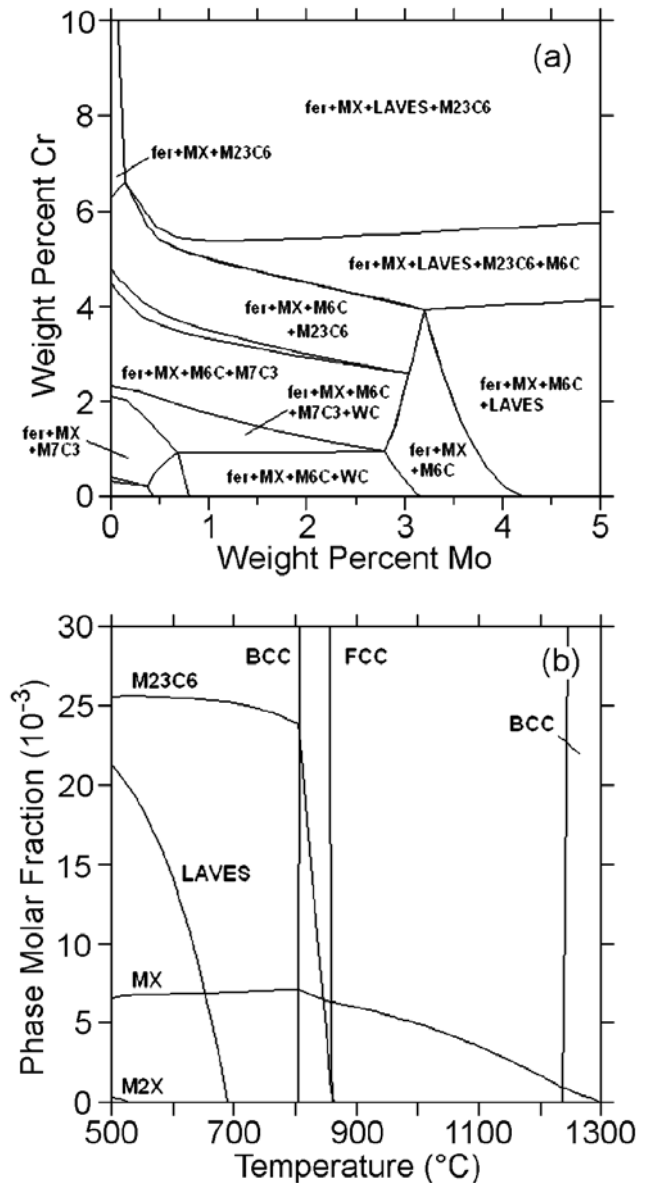


Fig. 11. The equilibrium phase diagrams for E911 steel: (a) mass fractions of secondary phases at 600°C, (b) temperature dependence on phase composition.

and the corrected time  $t_{fccorr}$  encompasses the time at the testing temperature during cyclic creep only, such that  $t_{fccorr}/t_f \geq 1$ . Thus, it is clear that the creep resistance of the investigated steels does not substantially deteriorate by cyclic thermal loading.

The question naturally arises regarding the cause of such behaviour. The creep resistance of 9%Cr creep-resistant steels can be influenced by (i) the strain fields associated with solid solution (solid solution hardening), (ii) the intragranular dislocation substructure distribution (dislocation hardening mechanism), (iii) grain boundary and sub-boundary hardening and (iv) intragranular particles, mainly MX precipitates

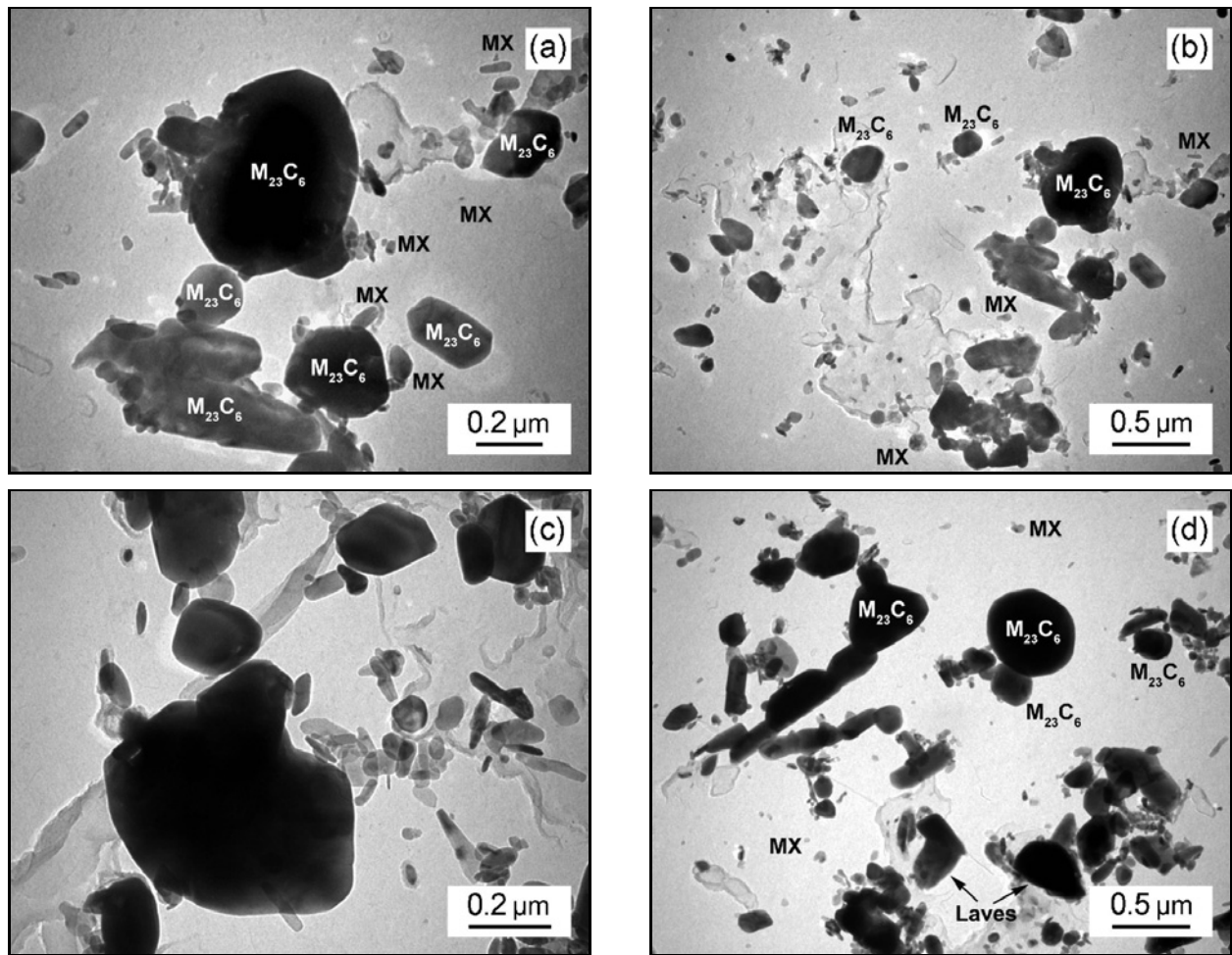


Fig. 12. TEM micrographs showing the precipitation in P91 steel: (a) and (b) monotonic creep, (c) and (d) cyclic creep (creep at 600 °C, 125 MPa, carbon replica).

(precipitation hardening) [6, 7, 13, 14, 41, 42]. As creep progresses, the dislocation substructure changes to form subgrains whose boundaries are stabilised by  $M_{23}C_6$  and possibly also by Laves phase particles [14, 43–45]. During creep exposure, the creep resistance becomes less dependent on resistance to the movement of individual dislocations through the matrix and more dependent on the resistance to subgrain growth through boundary migration [6, 43]. According to Abe [14], the sub-boundary hardening enhanced by the fine distribution of precipitates situated at boundaries gives the most important strengthening mechanism in the creep of tempered martensitic 9–12%Cr creep-resistant steels.

Finer subgrain size is a source of substructure hardening, as suggested Vastava and Langdon [46], and the growth of the subgrain size is a process of material softening and recovery. The model of the kinetics of subgrain growth due to recombination and migration of sub-boundaries was suggested by Straub et al. [47]. Furthermore, retarding the process of sub-

grain growth by blocking the sub-boundaries through precipitation is very important. Such a “pinning effect” of precipitation may represent one of the important roles of particle dispersion in steel. The results here suggest that the observed difference in the subgrain microstructure may be explained by possible additional precipitation reactions during intermittent heating. New precipitate secondary phase particles on subgrain boundaries and dislocations may block the migration of subgrain boundaries or the movement of mobile dislocations, which contribute to microstructural stability and consequently to the creep strength of the investigated steels. However, to complete the characterisation of the effect of intermittent heating in creep under cyclic thermal loading on subgrain size and precipitation, quantitative data on the size distribution of subgrains and secondary phase precipitates are strongly needed. Such a quantitative study is in progress at present.

Finally, the temperature changes consisting of cooling the high temperature component from the testing

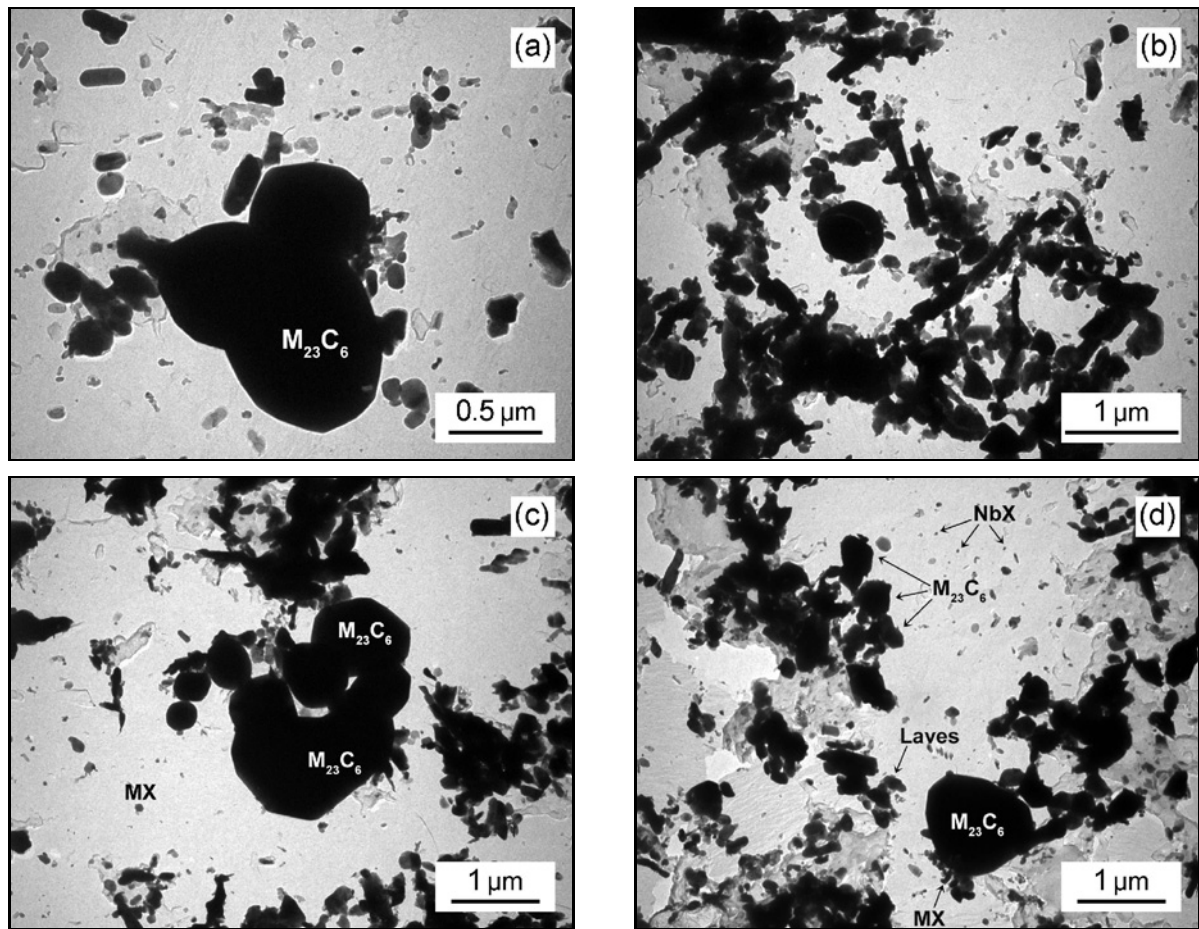


Fig. 13. TEM micrographs showing the precipitation in P92 steel: (a) and (b) monotonic creep, (c) and (d) cyclic creep (creep at 600 °C, 150 MPa, carbon replica).

temperature of 600 °C to room temperature and then heating it up again to the testing temperature may cause some additional strain generated by the thermal stresses created during the temperature changes and other degradation processes, such as high-temperature corrosion and oxidation, particularly at high temperatures. However, such phenomena seem not to affect the material laboratory behaviour during creep tests. Thus, provided that the microstructures of specimens subjected to both monotonic and cyclic thermal loading are relatively similar, there is no reason to expect substantially different creep behaviour in given steel during monotonic or cyclic creep tests.

## 5. Conclusions

1. The effect of cyclic thermal loading on the creep behaviour and microstructure evolution of three creep strength enhanced 9%Cr ferritic-martensitic P91, P92 and E911 steels was investigated. The thermal cycles consist of cooling the specimen from the creep testing temperature of 600 °C to room temperature

and then heating it up again to the testing temperature.

2. The thermal cycles have been repeated periodically after 24 h without removal of the applied stress during the whole creep test, continuing until the final fracture of the specimens. Standard creep tests at the same creep testing temperatures were performed simultaneously for comparison.

3. The results of the cycled and standard creep tests show no detrimental effect of intermittent heating on the creep behaviour of the specimens during the cycled tests.

4. Microstructural investigations revealed that there are no substantial differences regarding the types and chemical compositions of precipitating secondary phases after standard (monotonic) or cyclic creep in the three steels examined.

5. Provided that the microstructures of specimens subjected to both stationary and cyclic loading are relatively similar, there is no reason to expect substantially different creep behaviour for standard or cycled creep specimens.

6. Fractographic investigations of the creep frac-

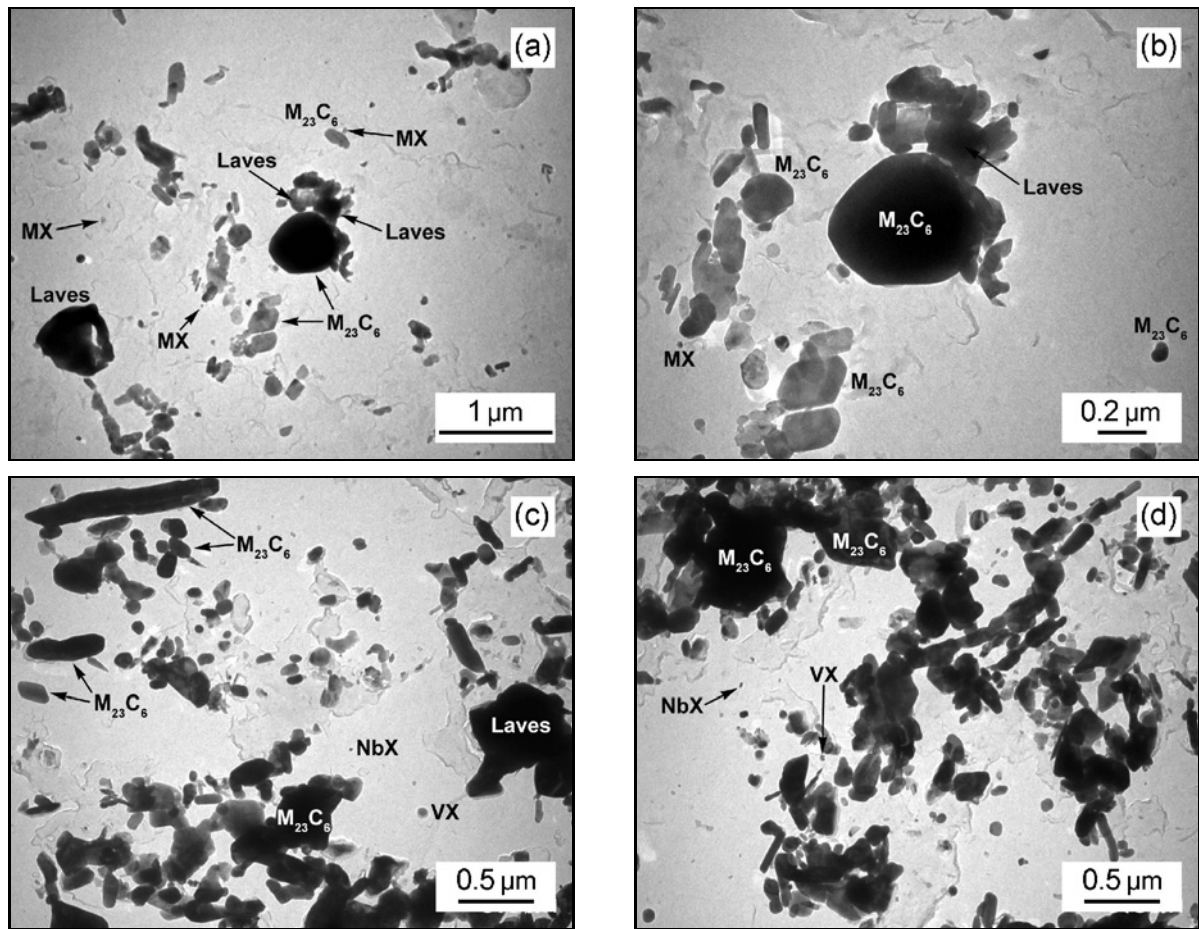


Fig. 14. TEM micrographs showing the precipitation in E911 steel: (a) and (b) monotonic creep, (c) and (d) cyclic creep (creep at 600 °C, 150 MPa, carbon replica).

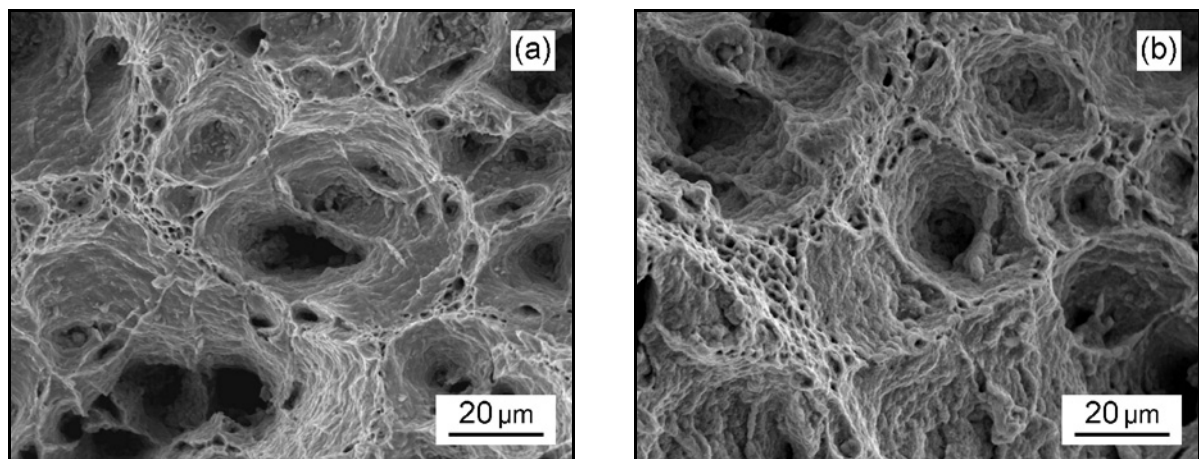


Fig. 15. SEM fractographs of P91 steel after creep at 600 °C and 125 MPa: (a) monotonic creep fracture surface, (b) cyclic creep fracture surface.

tured specimens of the examined steels revealed that the dominating creep failure is always of the ductile transgranular dimple fracture mode regardless of the creep testing history.

### Acknowledgements

We acknowledge financial support for this work provided by the Czech Science Foundation under the grant

project No. 16–09518S. Some experiments were realised using research infrastructure IPMINFRA supported by the Project LM2015069 financed by the Ministry of Education, Youth and Sports support of the Czech Republic.

## References

- [1] Shibli, A., Robertson, D. G.: In: Coal Power Plant Materials and Life Assessment – Developments and Applications. Ed.: Shibli, A. Cambridge, Woodhead Publishing 2014. ISBN 978-0-85709-5.
- [2] Akther, F., Hampson, S.: In: Proceedings of 10<sup>th</sup> Liege Conference: Materials for Advanced Power Engineering 2014. Eds.: Lecomte-Beckers, J., Dedry, M., Oakey, J., Kuhn B. Jülich, FZ Jülich 2014, p. 888.
- [3] Holdsworth, S. R.: Mater. High Temp., 28, 2011, p. 197. [doi:10.3184/096034011X13123676561681](https://doi.org/10.3184/096034011X13123676561681)
- [4] Keatley, P.: In: Coal Power Plant Materials and Life Assessment – Developments and Applications. Ed.: Shibli, A. Cambridge, Woodhead Publishing 2014. ISBN 978-0-85709-431-5.
- [5] Abe, F.: Mater. Sci. Eng. A, 319–321, 2001, p. 770. [doi:10.1016/S0921-5093\(00\)02002-5](https://doi.org/10.1016/S0921-5093(00)02002-5)
- [6] Sklenička, V., Kuchařová, K., Svoboda, M., Kloc, L., Buršík, J., Kroupa, A.: Mater. Charact., 51, 2003, p. 35. [doi:10.1016/j.matchar.2003.09.012](https://doi.org/10.1016/j.matchar.2003.09.012)
- [7] Ennis, P. J., Zielińska-Lipiec, A., Czyrska-Filemonowicz, A.: Mater. Sci. Technol., 16, 2000, p. 1226. [doi:10.1179/026708300101506993](https://doi.org/10.1179/026708300101506993)
- [8] Sklenička, V., Kloc, L.: In: Power Plant Life Management and Performance Improvement. Ed.: Oakey, J. E. Oxford, Woodhead Publishing Ltd. 2011. ISBN 978-1-84569-726-6.
- [9] Shibli, A.: In: Power Plant Life Management and Performance Improvement. Ed.: Oakey, J. E. Oxford, Woodhead Publishing Ltd. 2011. ISBN 978-1-84569-726-6.
- [10] Kimura, K., Takahashi, Y.: In: Proceedings of the 2012 ASME Pressure Vessel and Piping Conference. Toronto, ASME 2012, p. 309. [doi:10.1115/PVP2012-78323](https://doi.org/10.1115/PVP2012-78323)
- [11] Hasegawa, Y.: In: Coal Power Plant Materials and Life Assessment – Development and Applications. Ed.: Shibli, A. S. Woodhead Publishing Ltd. 2014. ISBN 978-0-85709-431-5.
- [12] Sakhtivel, T., Panneer Selvi, S., Laha, K.: Mater. Sci. Eng. A, 640, 2015, p. 61. [doi:10.1016/j.msea.2015.05.068](https://doi.org/10.1016/j.msea.2015.05.068)
- [13] Hald, J.: In: Materials for Ultra-Supercritical and Advanced Ultra-Supercritical Power Plants. Ed.: Di Gianfrancesco, A. Amsterdam, Elsevier Ltd. 2017. ISBN 978-0-08-100552-1.
- [14] Abe, F.: In: Materials for Ultra-Supercritical and Advanced Ultra-Supercritical Power Plants. Ed.: Di Gianfrancesco, A. Amsterdam, Elsevier Ltd. 2017. ISBN 978-0-08-100552-1.
- [15] Hätterstrand, M., Andren, H.-O.: Acta Mater., 49, 2001, p. 2123. [doi:10.1016/S1359-6454\(01\)00135-5](https://doi.org/10.1016/S1359-6454(01)00135-5)
- [16] Prat, O., Garcia, J., Rojas, D., Sauthoff, G., Inden, G.: Intermetallic, 32, 2013, p. 362. [doi:10.1016/j.intermet.2012.08.016](https://doi.org/10.1016/j.intermet.2012.08.016)
- [17] Barbadikar, D. R., Deshmukh, G. S., Maddi, L., Laha, K., Parameswaran, P., Ballal, A. R., Peshwe, D. R., Paretkar, R. K., Nandagopal, M., Mathew, M. D.: Int. J. Press. Vess. Pip. 132–133, 2015, p. 97. [doi:10.1016/j.ijpv.2015.07.001](https://doi.org/10.1016/j.ijpv.2015.07.001)
- [18] Wang, X., Wang, X., Li, H., Wu, H.-L., Ren, Y.-Y., Liu, H.-W., Liu, H.: Weld. World, 61, 2017, p. 231. [doi:10.1007/s40194-017-0424-2](https://doi.org/10.1007/s40194-017-0424-2)
- [19] Fournier, B., Sauzay, M., Pineau, A.: Int. J. Plast., 27, 2011, p. 1803. [doi:10.1016/j.ijplas.2011.05.007](https://doi.org/10.1016/j.ijplas.2011.05.007)
- [20] Li, M., Majumdar, S., Natesan, K.: J. ASTM International, 8, 2011, p. 1. [doi:10.1520/JAI103824](https://doi.org/10.1520/JAI103824)
- [21] Ando, M., Kanasaki, H., Date, S., Kikuchi, K., Satoh, K., Takasho, H., Tsukimori, K.: In: Proceedings of the 2012 ASME Pressure Vessels and Piping Conference. Toronto, ASME 2012, p. 323. [doi:10.1115/PVP2012-78402](https://doi.org/10.1115/PVP2012-78402)
- [22] Ando, M., Hasebe, S., Kobayashi, S., Kasahara, N., Toyashi, A., Ohmae, T., Enuma, Y.: Nucl. Eng. Des., 255, 2013, p. 296. [doi:10.1016/j.nucengdes.2012.10.016](https://doi.org/10.1016/j.nucengdes.2012.10.016)
- [23] Takahashi, Y., Gandy, D.: In: Proceedings of the 2011 ASME Pressure Vessels and Piping Conference. Toronto, ASME 2011, p. 227. [doi:10.1115/PVP2011-57976](https://doi.org/10.1115/PVP2011-57976)
- [24] Kim, W.-G., Park, J.-Y., Ekaputra, I. M. W., Kim, S.-J., Jang, J.: Mater. High Temp., 31, 2014, p. 249. [doi:10.1179/187864314Y.0000000021](https://doi.org/10.1179/187864314Y.0000000021)
- [25] Zhang, G., Zhao, Y., Xue, F., Wang, Z. J., Mei, L., Zhang, L., Zhou, C.: J. Press. Vess. Technol, 135, 2013, #041402. [doi:10.1115/1.4023424](https://doi.org/10.1115/1.4023424)
- [26] Takahashi, Y., Parker, J., Gandy, D.: In: Proceedings of the 7<sup>th</sup> Int. Conference Advances in Materials Technology for Fossil Power Plants. Eds.: Gandy, D., Shingledecker, J. Materials Park, ASM International 2014, p. 667. ISBN 13: 978-1-62708-060-6.
- [27] Gopinath, K., Gupta, R. K., Sahu, J. K., Ray, P. K., Gosh, R. N.: Mater. Des., 86, 2015, p. 411. [doi:10.1016/j.matdes.2015.07.107](https://doi.org/10.1016/j.matdes.2015.07.107)
- [28] Parker, J.: Trans. Indian Inst. Met., 69, 2016, p. 561. [doi:10.1007/s12666-015-0746-y](https://doi.org/10.1007/s12666-015-0746-y)
- [29] Zhang, W., Wang, X., Gong, X., Jiang, Y., Huang, X.: J. Mater. Sci. Technol., 33, 2017, p. 1540. [doi:10.1016/j.jmst.2017.09.006](https://doi.org/10.1016/j.jmst.2017.09.006)
- [30] Onizawa, T., Nagae, Y., Kato, S., Wakai, T.: J. Soc. Mater. Sci. Japan, 66, 2017, p. 122. [doi:10.2472/jsms.66.122](https://doi.org/10.2472/jsms.66.122)
- [31] Kim, W.-G., Park, J.-Y., Ekaputra, L. M. W., Kim, S.-J., Jang, J.: Nucl. Eng. Technol., 49, 2017, p. 581. [doi:10.1016/j.net.2016.11.007](https://doi.org/10.1016/j.net.2016.11.007)
- [32] Pohja, R., Holmström, S., Auerkari, P., Numela, A.: Mater. High Temp., 13, 2017, in press. [doi:10.1080/0960349.2017.13837.10](https://doi.org/10.1080/0960349.2017.13837.10)
- [33] Jarvis, M., Raddings, T.: In: CCGT Plant Components – Development and Reliability. London, IMechE 1999.
- [34] Mayer, K. H., Masuyama, F.: In: Creep Resistant Steels. Eds.: Abe, F., Kern, T.-U., Viswanathan R. Cambridge, Woodhead Publishing Ltd. 2008. ISBN 978-1-84569-178-3.
- [35] Berger, C., Beech, S. M., Mayer, K.-H., Staubli, M., Thornton, D.: In: Proceedings of the 1993 International Joint Power Generation Conference. Kansas City, ASME 1993, p. 63. ISBN 079180996 X.
- [36] Hald, J.: Int. J. Press. Vess. Pip., 85, 2008, p. 30. [doi:10.1016/j.ipvp.2007.06.010](https://doi.org/10.1016/j.ipvp.2007.06.010)

- [37] Hald, J., In: Modelling of Microstructural Evolution in Creep Resistant Materials. Eds.: Strang, A., McLean, M. London, IOM Communications Ltd. 1999. ISBN 1-86125-097-5.
- [38] Strang, A., Vodarek, V.: Mater. Sci. Technol., 12, 1996, p. 552. [doi:10.1179/mst.1996.12.7.552](https://doi.org/10.1179/mst.1996.12.7.552)
- [39] Sawada, K., Kushima, H., Kimura, K., Tabuchi, M.: ISIJ International, 47, 2007, p. 733. [doi:10.2355/isijinternational.47.733](https://doi.org/10.2355/isijinternational.47.733)
- [40] Sklenicka, V.: In: Modelling of Microstructural Evolution in Creep Resistant Materials. Eds.: Strang, A., McLean, M. London, IOM Communications Ltd. 1999. ISBN 1-86125-097-5.
- [41] Maruyama, K., Sawada, K., Koike, J.: ISIJ International, 41, 2001, p. 641. [doi:10.2355/isijinternational.41.641](https://doi.org/10.2355/isijinternational.41.641).
- [42] Čadek, J.: Creep in Metallic Materials. Amsterdam, Elsevier Science Publishers 1988.
- [43] Orlová, A., Buršík, J., Kuchařová, K., Sklenička, V.: Mater. Sci. Eng. A, 245, 1998, p. 39. [doi:10.1016/S0921-5093\(97\)00708-9](https://doi.org/10.1016/S0921-5093(97)00708-9)
- [44] Hasegawa, Y., Muraki, T., Ohgami, M., Mimura, H.: Key Eng. Mater., 171–174, 2000, p. 427. [doi:10.4028/www.scientific.net/KEM.171-174.427](https://doi.org/10.4028/www.scientific.net/KEM.171-174.427)
- [45] Korčáková, L.: Microstructure Evolution in High Strength Steel for Power Plant Application: Microscopy and Modelling. [Ph.D. Thesis]. Lyngby, Technical University of Denmark 2002.
- [46] Vastava, R. B., Langdon, T. G.: In: Advances in Materials Technology in the Americas Volume 2. New York, ASM International 1980.
- [47] Straub, S., Meier, M., Ostermann, J., Blum, W.: VGB Krafttechnik, 73, 1993, p. 744.